AIAA 2001-0787
INTERPRETATION OF OPTICAL EMISSIONS FOR SENSORS IN LIQUID FUELED COMBUSTORS

M. R. Morrell, J. M. Seitzman, M. Wilensky,
E. Lubarsky, J. Lee, and B. Zinn
Georgia Institute of Technology
Atlanta, GA

39th Aerospace Sciences Meeting & Exhibit
January 8-11, 2001 / Reno, NV

AIAA-2001-0787

INTERPRETATION OF OPTICAL EMISSIONS FOR SENSORS IN LIQUID FUELED COMBUSTORS

M. R. Morrell*, J. M. Seitzman†, M. Wilensky‡, E. Lubarsky§, J. Lee‡, and B. Zinn**

Georgia Institute of Technology
Aerospace Combustion Laboratory
School of Aerospace Engineering
Atlanta, GA 30332-0150

Abstract

The optical emissions from a turbulent, nonpremixed, liquid fueled (n-heptane) combustor were investigated using two optical imaging systems: a high spectral resolution (~0.3 nm), single wavelength system; and a low resolution (~5 nm), multi-wavelength system intended to mimic the response of a practical sensor. The goal was to develop signal interpretation strategies that would allow an optical sensor system to monitor needed properties in liquid-fueled combustors and engines. The research focused on the chemiluminescent emissions from OH*, CH*, and C_2*. Data were acquired for a range of fuel and air flow rates (equivalence ratios 0.6-1.3), and for radial slices through the nominally axisymmetric combustor over the complete combustor length.

Without correction, both OH* and CH* emission were found to be good indicators of heat release rate only over a narrow band of lean equivalence ratios. In addition, OH* provides information on the post-combustion zone conditions. A nearly linear relationship was found between the overall equivalence ratio of the combustor and the ratio of the emission integrated over the combustor volume from two radical species, with the ratio C_2*/OH* exhibiting the greatest sensitivity. The correlation was also applied to estimate the radially averaged equivalence ratio of the reaction zone along the length of the combustor. With the multi-wavelength sensor set to simultaneously monitor the broadband background from the flame, its background corrected output agreed well with the high spectral resolution results, suggesting that a properly designed optical sensor system would be capable of determining local combustor conditions such as reaction zone equivalence ratio and heat release rate.

Introduction

The advent of digital engine control units in modern aircraft and power generation gas turbine engines, together with the extraordinary growth in microprocessor capacity, provides new opportunities to improve the performance, flexibility, and reliability of these and other modern combustion systems. For active engine control using state feedback, reliable and versatile sensors are required. For control of the combustor itself, there is a need for sensors that can respond to fluctuations in the heat release rate (or reaction rate) in the combustor, variation in the local (reaction zone) fuel-air ratio, temperature distribution at the combustor exhaust, and the absence or presence of the flame. Other potential applications for such sensors are waste incineration control, ground propulsion internal combustion engines, engine/combustor health condition monitoring, ignition or fire detection, and combustion diagnostics.

In current turbine engine systems, thermocouples are most frequently used to provide this sort of feedback. For example, a limited thermocouple array is often located between the high and low pressure turbines to provide engine health condition monitoring and ignition detection. This thermocouple array is severely limited in its capability due to the significant time lag between events occurring in the combustion chamber and the effects of those events reaching the thermocouple. Furthermore, the presence of the high pressure turbine upstream of the thermocouple makes it difficult to reconstruct the flow pattern and profile in the combustion chamber. Direct monitoring of pattern and profile factors at the combustor exit would be desirable; however, thermocouples are not a viable

*Graduate Research Assistant, Student Member AIAA
†Associate Professor, Senior Member AIAA
‡Graduate Research Assistant
§Research Engineer, Member AIAA
**David S. Lewis Jr. Chair, Regents Professor, AIAA Fellow

option due to the high temperatures. A further limit of thermocouples is that they are capable of collecting information only in their immediate vicinity.

As an alternative, optical sensors offer the benefit of being able to gather data from extremely hostile environments (e.g., the combustion zone), and to do so over large regions of space. For example, limited capability optical sensors are commonly employed as flame detectors in many ground-based combustion systems. Passive optical sensors offer the further advantage of simplicity, which makes them an attractive candidate. High temperature, rugged solid-state sensors (e.g., photodiodes) with fast response, low power requirements, spectrally selectable design, and access to the ultraviolet are now being developed.[1-2] With the rapidly growing capability of these technologies for sensor hardware, there is an increased interest and need to develop data interpretation strategies that will allow optical flame emission data to be converted to meaningful combustor state information, e.g., fuel-air ratio, reaction rate, and temperature.

Optical Flame Emission

The visible and ultraviolet optical signature from the combustion of hydrocarbon fuels and air typically consists of a combination of molecular radiation from electronically excited species and luminosity from particles such as soot. The electronically excited molecules can be created through either chemical reactions or thermal collisions. Radiation from chemically produced states is denoted as chemiluminescence and is indicated in this paper with an asterisk, *. Table 1 lists visible and ultraviolet wavelengths associated with chemiluminescence for various combustion radicals and products.

Table 1. Flame emission wavelengths for common combustion radicals and products.

Species	Wavelength [nm]
OH*	306-315
NH*	336
CN*	359, 386
CH*	390, 431
C_2*	469-473, 510-516
CH_2O*	395, 423
CO_2*	broadband

The current and previous studies have primarily focused on radiation from OH*, CH*, and C_2*. CH* and C_2* can provide easily observable signals, as they are strong emitters and their radiation is spectrally resolved (i.e., spectrally narrow), though their signals can be obscured in some flames due to broadband CO_2*[3] and soot blackbody radiation[4]. OH* is attractive because the reduced blackbody radiation (from particles and walls) in the ultraviolet, even in very luminous flames, increases its observability.

Since the chemiluminescence from these radicals is the result of chemical reactions[5] and their life times are short compared to fluid mechanical (e.g., convective) time scales, radical chemiluminescence provides information on the state of the reaction zone in a combustor. For example, CH* is often used as a measure of heat release rate. Correlations between OH* chemiluminescence and flame temperature have also been investigated.[6,7] Keller and Saito[8] used OH* to measure burning rate and to demark the reaction zone in a pulse combustor. Recently, Lawn[9] used an optical system with two intersecting lines-of-sight to determine the correlation between OH* and the instantaneous heat release. Kojima *et al.*[10] and Ikeda *et al.*[11] used a spatially resolved system to measure OH* and C_2* to measure flame front movement. Roby *et al.*[12] tested the response time of chemiluminescent emissions for looking for flame detection.

The effect of equivalence ratio (ϕ) on chemiluminescence has also been studied. Dandy and Vosen[13] conducted experimental studies and constructed models of OH* in lean methane-air flames and determined an exponential dependence of OH* on ϕ over the range 0.65 to 0.90. Samaniego *et al.*[3] conducted a numerical investigation focused on CO_2* and OH* chemiluminescence in lean hydrocarbon flames to determine their dependence on equivalence ratio, as well as dilution and strain-rate. Experiments in simple hydrocarbon gas flames have also examined the dependence of ratios of chemiluminescence from different species on equivalence ratio. Roby *et al.*[7] found the ratios OH*/CH* and C_2*/CH* to be nearly linear functions of equivalence ratio. Kojima *et al.*[14] recently published results of a similar investigation using a spatially resolved system in which OH*/CH* was used to determine the local flame stoichiometry of the reaction zone of a laminar, premixed, methane-air flame over a range ϕ=0.9-1.5.

Little previous work has investigated chemiluminescence interpretation for equivalence ratio or temperature sensing in liquid-fueled combustion systems. Similarly, nonpremixed or partially premixed combustion has also been largely neglected. Since aeropropulsion systems, and many ground-based combustors, employ liquid fuels, there is a clear need to examine these issues in liquid-fueled combustion.

Experiment Description

Combustor

This research was conducted on a liquid-fueled, turbulent combustor[15] illustrated in Figure 1 and pictured in 2. Pressurized liquid fuel, n-heptane (C_7H_{16}), is supplied to the bottom of the combustor through a modified pressure-atomizer. The atomizer is controlled by a magnetostrictive actuator that adjusts the position of a pintle (also enabling the fuel flow to be pulsed at up to 5 kHz). One-third of the airflow is injected through four tangential air jets, further atomizing the fuel and introducing swirl to the flow. The remaining two-thirds of the air is supplied to the flame as an annular stream entering around the periphery of the conical, stainless steel flameholder. The primary liquid-air mixture, which passes through the flameholder, mixes with the secondary airflow downstream.

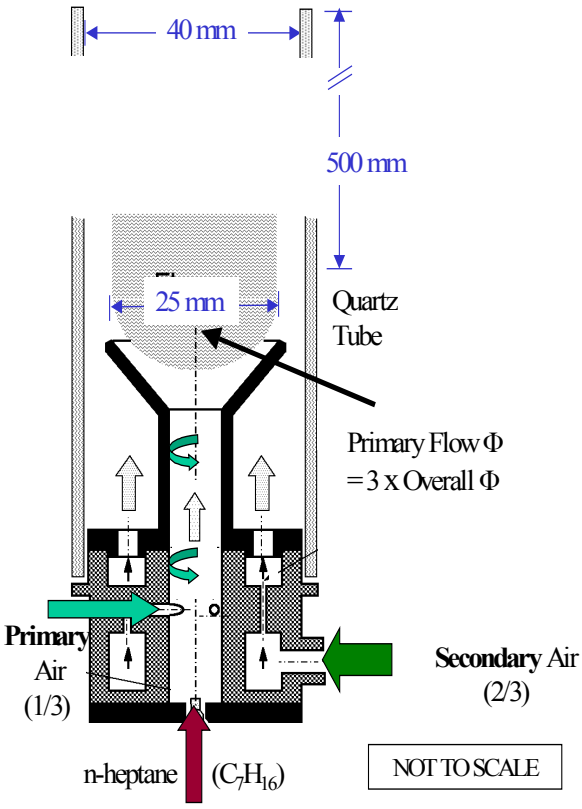

Figure 1. Schematic of liquid-fueled combustor.

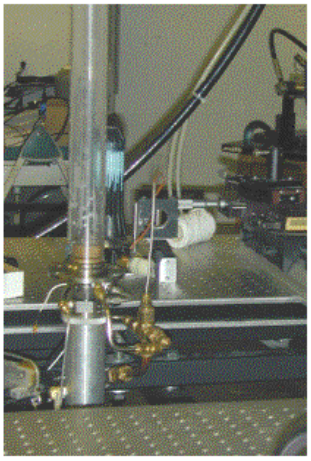

Figure 2. Picture of the liquid-fueled combustor.

A quartz tube extends upward from the combustor base, providing optical access to the flame with high transmission of wavelengths from the ultraviolet to the infrared. The tube has a 42 mm (1.6 in) inner diameter, is 1.5 mm (0.06 in) thick, and is 500 mm (20 in) long. The maximum airflow rate is ~15 g/s and the maximum fuel flow rate is ~1 g/s. The lean and rich stability limits of the flame are at overall equivalence ratios of ~0.6 and ~1.35. Since only one-third of the air is initially mixed with the fuel, the primary flow equivalence ratio is roughly 3 times that of the global equivalence ratio. The air entering the combustor can be preheated in an electrical resistance heater to a maximum of ~300°C.

The combustor is mounted to a motorized traverse for automated control of its vertical position, allowing the optical systems to remain stationary while the combustor is traversed during data taking. The vertical traverse allows 260 mm of the flame to be observed by the optical system, and takes roughly 10 seconds to complete a bottom to top traverse. The location of the combustor is monitored by recording a voltage signal from the traverse stepper motor controller using LabView software running on lab computer.

Monochromator System

Two optical detection systems were used to analyze the radiative emissions from the combustor. The first system was only capable of recording single-point, single wavelength data. Light from the central portion of the combustor was imaged by a lens onto the entrance slit of a monochromator, the selected wavelength detected by a photomultiplier (PMT), and the PMT voltage output recorded on a computer (Figure 3).

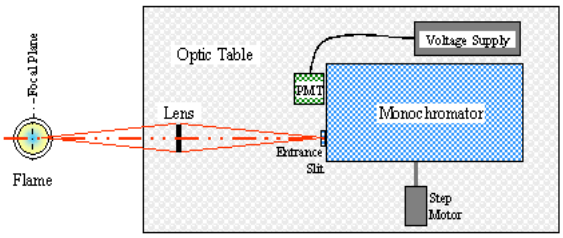

Figure 3. Schematic of monochromator (single-point, single-wavelength) imaging system.

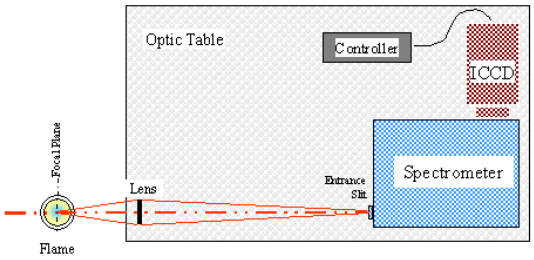

Figure 4. Schematic of spectrometer (single-point, multi-wavelength) spectral imaging system.

The fused silica, plano-convex, spherical lens used had a 20 cm focal length and a 5 cm diameter. The lens was positioned to provide unity magnification (1:1 imaging), and an aperture next to the lens reduced its effective diameter to 4 cm in order to match the monochromator's f-number of f/10. The Jarrell Ash 82-020 Monochromator contained a 1200 grooves per mm holographic gratings. The monochromator entrance slit was set at 0.5 mm by 3 mm, defining the lateral and axial resolution of the system, that is all data points represent a 0.5 mm by 3 mm slice of flame at the center of the combustor (the focal plane of the lens). In the depth direction, the emissions were integrated along a thin cone parallel to the optical axis. The exit slit was set to achieve roughly 0.3 nm resolution. The monochromator was able to scan the full spectrum of interest (280 to 550 nm) in 145 seconds.

Spectrometer System

The second system was capable of recording single-point, multiple wavelength data. The same general system layout was used, but with an imaging spectrometer and intensified CCD (ICCD) camera replacing the monochromator and PMT (Figure 4). The same fused silica lens was used, but at a magnification of 3:1 (object size: image size). This system was based on an Acton Spectra-Pro 300i imaging spectrometer with a 300 grooves per mm grating, allowing the simultaneous capture of emission spectra from the full spectrum of interest (280 – 550 nm). In order to mimic the anticipated resolution of practical engine optical sensors, the resolution of the spectrometer was set at ~5 nm through control of the entrance slit width.

The PI-MAX ICCD located at the exit plane of the spectrometer is equipped with a 25 mm intensifier and a 1024×256 (26 μm) pixel CCD. Overall, the ICCD could simultaneously acquire spectra from a vertical region in the flame of ~16 mm. To decrease data acquisition time, the top and bottom regions of the CCD were not read and the data from the remaining area on the CCD was "binned" into nine vertical regions (rows), with each row representing a 1 mm tall region in the flame. The intensifier was gated for 250 μs at a repetition rate of 120 Hz, while the CCD was integrated for 85 ms. Thus 10 images were averaged on each CCD exposure (with an overall temporal resolution of 85 ms). The image acquisition rate was 8.1 Hz, based on a readout time of 27 ms and an overall time between images of 112 ms. Images were acquired while the combustor was continuously traversed downward at a rate of 26 mm/s producing a motion of ~3 mm between successive images.

Results

Overall Spectrum and Background

A high-resolution investigation of the visible and ultraviolet spectrum (300 nm to 525 nm) from the n-heptane fueled combustor was conducted with the monochromator at a height ~20 mm above the flameholder (see Figure 5). Due to the time required to scan across the spectrum (145 seconds), the emission spectra are sensitive to variations in the flame caused primarily by small variations in the fuel flow rate, and also by combustor instabilities.

The top chart in Figure 5 shows the full spectrum of interest. As expected, the primary sources of emissions are OH*, CH*, and C_2*. The relative effect of equivalence ratio is indicated in the lower portion of the figure. As the overall ϕ changes from lean to rich, the OH* emission decreases slightly, CH* emissions increases slightly, and C_2* emissions increases significantly.

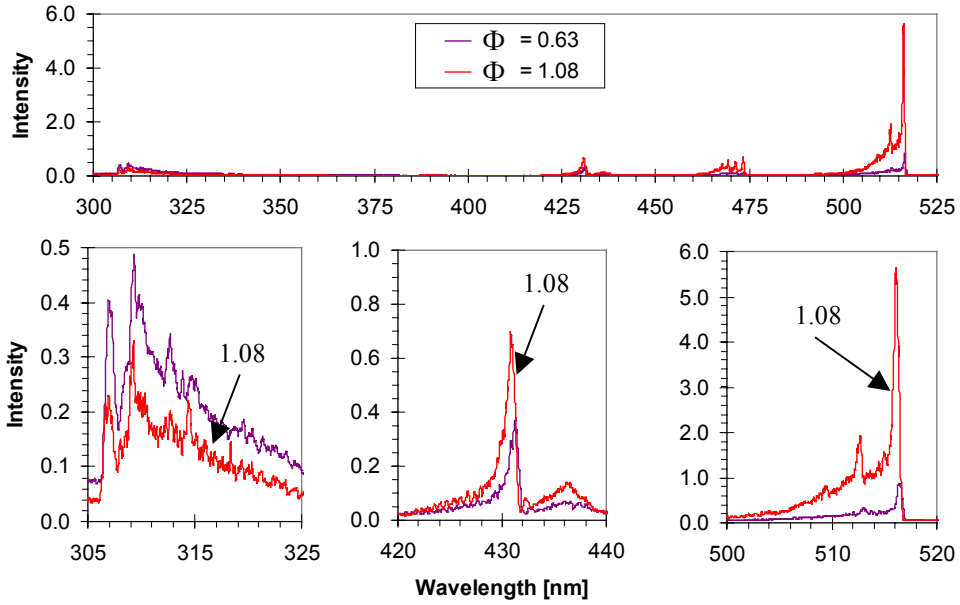

Figure 5. Emission spectra acquired by the monochromator system. (top) Scans from 300 nm to 525 nm, and (bottom) close-ups of (left) OH*, (center) CH*, and (right) C_2* spectra.

Figure 6 presents similar data taken with the spectrometer system at a much lower resolution, more like what might be expected from a realistic sensor. The spectrum displays the same characteristics, but with lower, broader, and smoother spectral features. The reduction in the peak intensities makes the broadband background radiation much more apparent.

This broadband background radiation is distinct from the camera background, which is recorded by the pixels at the two extreme ends of the spectrum that are beyond the edge of the active region of the intensifier and therefore are blocked from receiving any light. The broadband background only occurs when the combustor is operating and comes directly from the combustor. Spectral filters were placed in front of the spectrometer to rule out spectral aliasing/ghosting inside the spectrometer, which occurs when light at one wavelength appears to be coming from another wavelength due to optical deficiencies and aberrations within the spectrometer. The background also disappears when the spectrometer's line of sight is above the flame, thus indicating that the background is not from the glowing (red) quartz tube. As seen in Figure 6, the background signal is also a function of equivalence ratio, generally decreasing for progressively richer systems. These observations are in accordance with the expected behavior of CO_2* and its broadband radiation spectrum.[3]

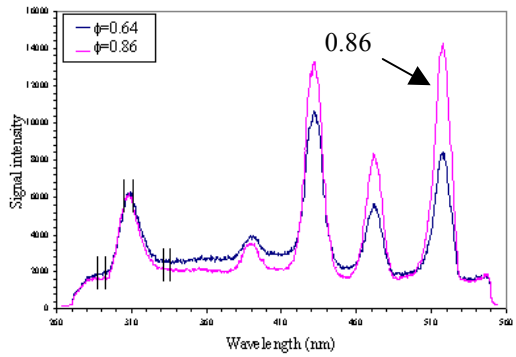

Figure 6. Emission spectra acquired by the spectrometer system. These results are averaged over 6 mm of flame height.

To isolate the radiation from OH*, CH*, and C_2*, the interference from the background was removed from each molecular emission peak by first integrating the signal over a small spectral region approximately 4 nm wide centered at the peak. Then the background was estimated from the average of the integrated signal from two similar-sized regions on either side of the peak. These areas are indicated on Figure 6 for OH* by vertical bars. The background adjusted radical emission was found by taking the difference between the peak signal and the average background. This *adjusted* data is used throughout this paper for all spectrometer-produced data, unless otherwise indicated.

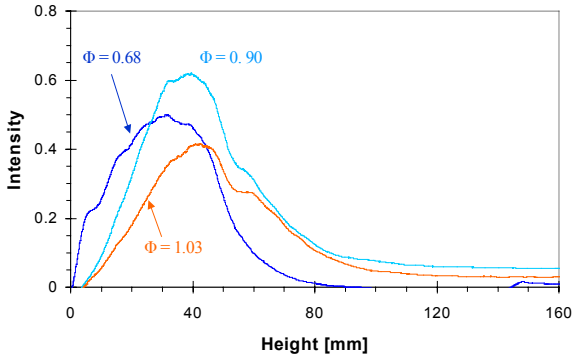

Figure 7. Vertical profile of OH* emission at various equivalence ratios by changing the fuel flow rate while keeping the air flow constant.

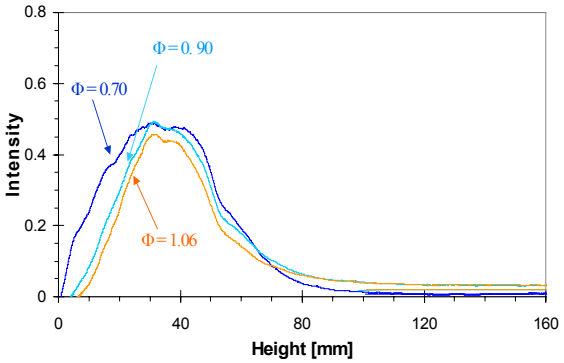

Figure 8. Vertical profile of OH* emission at various equivalence ratios by changing the air flow rate while keeping the fuel flow constant.

Vertical Emission Profiles

The vertical profiles of the optical emissions along the flow axis of the combustor were gathered by traversing the combustor while keeping the optical system fixed. This procedure requires approximately 10 seconds, so variations in the combustor operating conditions (primarily fuel flow) or episodes of combustion instability can be an issue. When this was observed during experiments, the results were discarded. Also, several experiments were performed at each combustor condition to ensure repeatability.

Figures 7 and 8 show OH* vertical emission profiles for various equivalence ratios. The equivalence ratio was altered either by varying the air flow while holding the fuel flow rate constant (Figure 7), or by varying the fuel while keeping the air flow unchanged (Figure 8). Similar to the findings from the flame spectra, the OH* emission profiles show a dependence on equivalence ratio. As might be expected in this non-premixed (or partially premixed) combustor, the radical chemiluminescence is also a function of downstream location in the combustor, with the peak in the chemiluminescence profile occurring in the region of maximum fuel consumption.

For the OH* profiles, the peak intensity generally increases and its location moves further downstream as the equivalence ratio is raised from the leanest case until $\phi \cong 0.9$. Above this value, the peak signal decreases, while the peak location continues to shift upstream. This trend is much more pronounced when the fuel flow rate is varied (Figure 8), since an increase in the total fuel consumed will also lead to a relative increase in the total radical production, and therefore the amount of chemiluminescence.

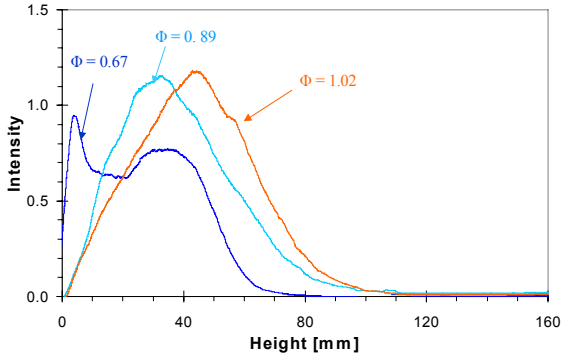

Figure 9. Vertical profile of CH* emissions at various equivalence ratios by changing the fuel flow rate while keeping the airflow rate constant.

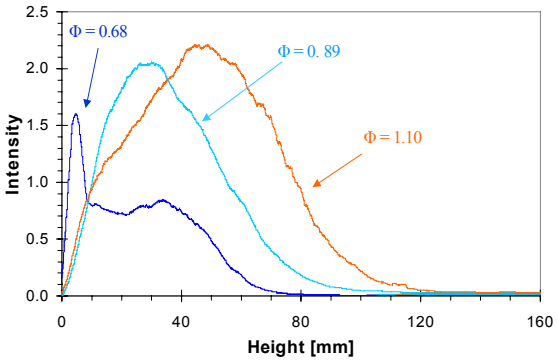

Figure 10. Vertical profile of C_2* emissions at various equivalence ratios by changing the fuel flow rate while keeping the air flow rate constant.

The peak emission signal location varies from 30 to 40 mm while the overall flame length varies from 75 to 100 mm. Note, however, that the OH* emission does not disappear (or more correctly does not decrease to the background level) above the active combustion zone , as do CH* and C_2* (see Figures 9 and 10). This residual OH* emission may result from a secondary reaction zone with an altered chemical pathway that avoids the CH* and C_2* production reactions. It is also

likely due to the higher equilibrium levels of OH in the flame products, compared to CH and C_2, and the resulting thermally produced OH*. At lean conditions, the equilibrium levels of OH are low due to the scarcity of hydrogen, and, at rich conditions, the equilibrium levels of OH are low due to the scarcity of oxygen. The analytically calculated equilibrium concentrations of OH are plotted in Figure 11 As can be seen, the equilibrium concentrations of OH are an order of magnitude higher at equivalence ratios from 0.8 to 1.1 than at 0.6 or 1.2. The OH* tails in Figure 7 and Figure 8 follow the same trend as the equilibrium OH concentrations, with the largest OH* signal from experimental runs with equivalence ratios of 0.8 to 1.0.

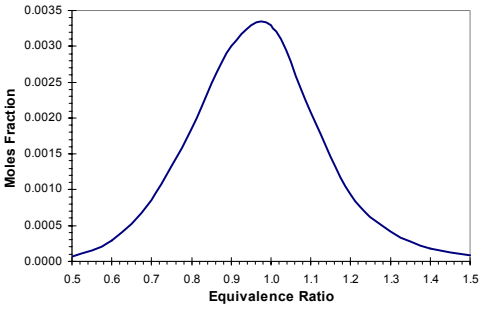

Figure 11. Calculated equilibrium mole fraction of OH for an n-heptane / air flame.

It should also be noted that the combustor employed here has a distinct feature when operating under very lean conditions, especially for high overall flow rates. For these conditions, there is an initial reaction zone within the flameholder, as evidenced by a small peak in the CH* and C_2* signals just above the flameholder. This occurs because the primary air is varied along with the total air flow (~33% of the total air). For most conditions, the equivalence ratio inside the flameholder is beyond the rich flammability limit. At the leanest overall conditions, however, the primary mixture becomes flammable.

Height Integrated Emissions

One of the primary goals of this effort was to examine the relationship between the chemiluminescence signature of the liquid-fueled combustor and the equivalence ratio. Since the present liquid-fueled combustor (like most such systems) is not completely premixed, the local equivalence ratio is not easily determined. The overall equivalence ratio, on the other hand, is readily available and can be used to compare to the overall, spatially integrated emission from the flame. A measure of the volume-integrated emission can be found by integrating, over the combustor length, the already radially integrated emission profiles of the type shown in Figures 7-10. These integrated results should be nearly proportional to the total radical emission from the combustor. A more accurate value of the total integrated emission would require an azimuthal integration with a radial correction.

Figure 12 shows the integrated emission results for a variety of equivalence ratios, obtained by varying either the fuel or air flow. Based on the assumption, noted previously, that the integrated chemiluminescence should scale with the total amount of fuel burned, the integrated emission results have been normalized by the fuel flow rate associated with each data point. Thus, the data shown in Figure 12 are more properly characterized as the integrated emission intensity per fuel mass.

Except for the C_2 results in the stoichiometric and rich regions, the normalization by fuel flow properly brings the different data sets into agreement. The results include the following trends. First, the OH* emission generally decreases as the equivalence ratio is increased, though it is nearly constant for $\phi<0.8$. Second, CH* emission is nearly constant from $0.75<\phi<0.9$, and decreases outside this range. Third, C_2* emission rises with increasingly rich mixtures, with the most rapid rise for $\phi<0.9$-1. The results for the leanest equivalence ratios ($\phi<0.7$) must be looked at with caution, however, as the results presented in the previous section indicate some amount of combustion occurring within the optically inaccessible flameholder. The total measured emissions from the flame for these lean conditions should thus be less than the actual emissions. Based on the vertical profiles, we expect C_2* to be most affected and OH* least affected by this phenomenon.

While CH* chemiluminescence is often used as an indicator of the heat release or heat release rate in the flame, the current results show that the CH* emission normalized by fuel burned is not a constant, except in a small equivalence ratio range (0.75-0.9). In order to accurately use CH* as a quantitative marker of heat release, it is clear that the equivalence ratio of the region producing the CH* emission must also be known. OH* emission has also been suggested previously as a heat release monitor. Based on the results from the liquid-fueled combustor, OH* would appear to be a reasonable marker of total heat release for lean conditions ($\phi<0.9$), but for near stoichiometric or rich conditions, the equivalence ratio must again be known.

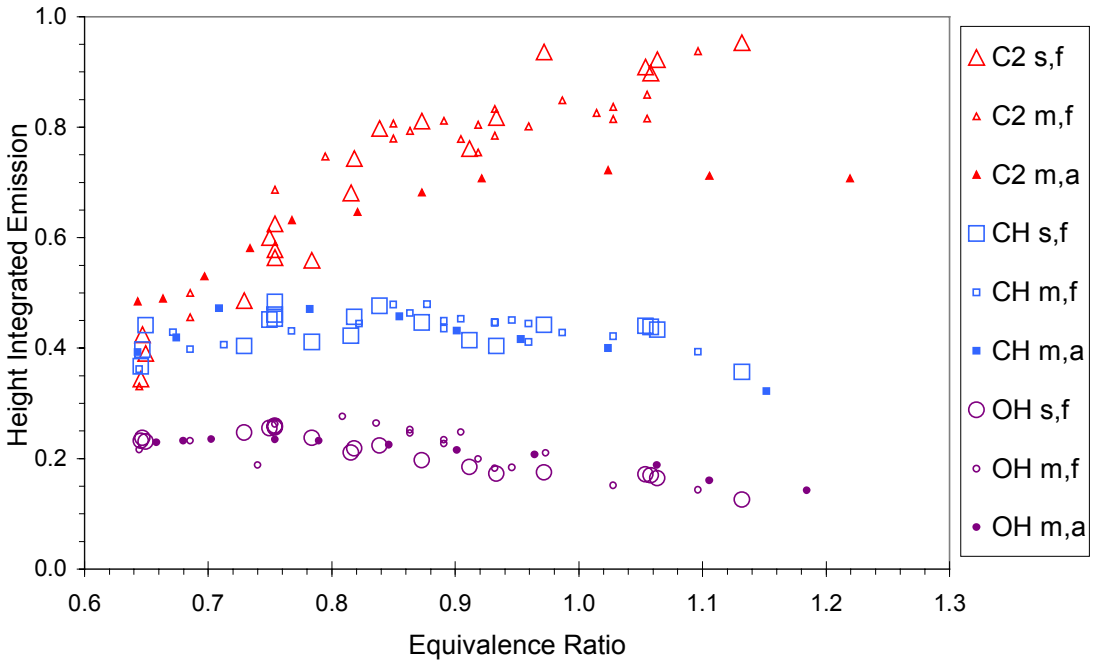

Figure 12. Variation of the vertically integrated radical emission signals as a function of equivalence ratio. Large open symbols represent data collected with the imaging spectrometer while varying fuel flow rates. Small symbols represent data collected by the monochromator, with open symbols for varying fuel flow rates and filled symbols for varying air flow rates.

Ratios of Radical Emissions

The results presented above indicate that the fuel-normalized and vertically integrated emission of each radical species varies uniquely with overall equivalence ratio. It should be possible, therefore, to combine the measurements from multiple species to remove the dependence on the fuel consumption rate and obtain a measure of equivalence ratio. A ratio of the integrated emission signals is a simple approach, and such results are shown in Figure 13 for three ratios: C_2*/OH*, CH*/OH*, and C_2*/CH*. In all three cases, the figure indicates a roughly linear response between overall equivalence ratio and integrated emission ratio. The C_2*/OH* ratio shows the greatest sensitivity, and thus appears to be the best candidate for determining equivalence ratio. The CH*/OH* and C_2*/CH* data have roughly the same slope sensitivity, each about half that of their product, C_2*/OH*.

Figure 14 shows a comparison of the C_2*/OH* data acquired with both detection systems. The spectrometer system more closely mimics the behavior of a realistic sensor, in that the data from the different emission bands is acquired simultaneously, and its spectral resolution is closer to what would be expected from a photodiode/filter based system. Results are shown for the "raw" spectrometer data, and data corrected to account for the broadband background.

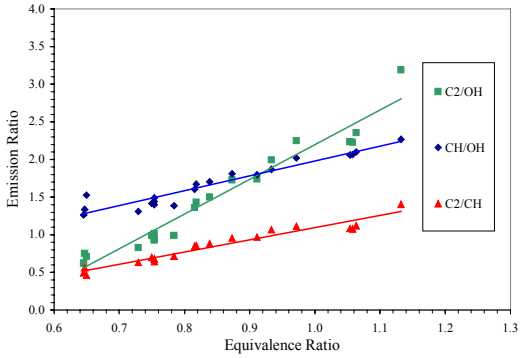

Figure 13. Dependence of the ratios of vertically integrated emissions of radical species on the overall equivalence ratio. Linear approximations of the data have been superimposed.

The background adjustment increases the C_2*/OH* sensitivity to variation in the equivalence ratio. While the higher resolution of the monochromator system results in much better signal-to-background data, as observed in Figures 5 and 6, the agreement between the monochromator results and the background adjusted spectrometer data is excellent, indicating that there is

no significant loss in sensitivity for a realistic sensor bandwidth when the background is properly corrected. Therefore, this capability should be considered in the design of a practical sensor.

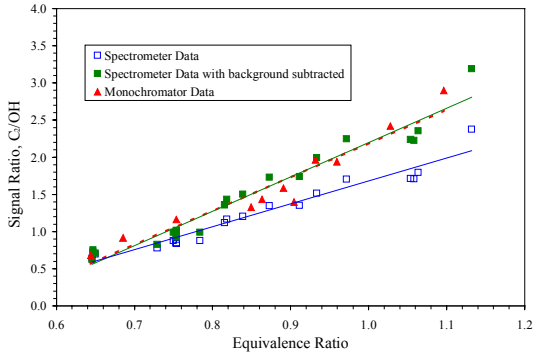

Figure 14. Comparison of results from the spectrometer and monochromator systems of the C_2*/OH* emission ratio dependence on equivalence ratio.

For the data shown in Figures 13-14, each equivalence ratio result was obtained from only one or two combinations of fuel and air flow. As indicated previously (Figures 7-10), the combustion process is also a strong function of overall flow rate in the combustor. This is because variations in the flow rate change the flame length, the liquid fuel atomization, and the intensity of mixing in the lower portion of the burner due to changes in the swirl flow. Therefore, further tests were conducted to determine whether the relationship shown in Figure 14 has some global validity over a larger range of conditions.

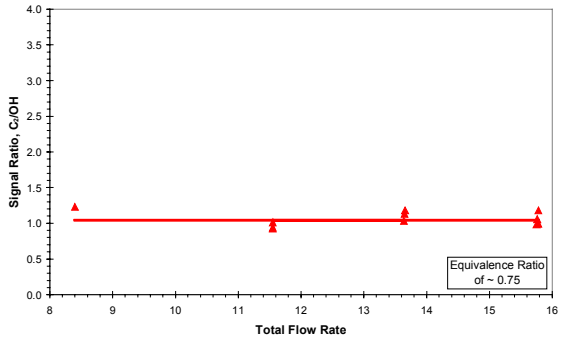

Figure 15. Effect of total mass flow rate on the C_2*/OH* emission ratio, for a fixed overall equivalence ratio of 0.75. The dashed horizontal line is the emission ratio value expected from the linear correlation shown in Figure 14.

Figure 15 shows results for a single equivalence ratio obtained for a wide range of total mass flow rates. The C_2*/OH* integrated emission ratio is not visibly sensitive to the overall mass flow rate of the combustor; the variation with mass flow rate seen here is comparable to the repeatability of the data for a fixed mass flow rate. Based on the linear fit shown in Figure 14, the variation in the C_2*/OH* ratio over the range of mass flow rates measured would correspond to a change in equivalence ratio of only 0.02. Similar behavior was found for the CH*/OH* and C_2*/CH* ratios.

A second series of tests was performed to determine the effect of the inlet air temperature on the emission ratio. Using an electric air preheater, results were obtained for inlet air temperatures ranging from 298 K to 473 K. The results are illustrated in Figure 16, which indicates the correlation is relatively insensitive to moderate variations in initial temperature.

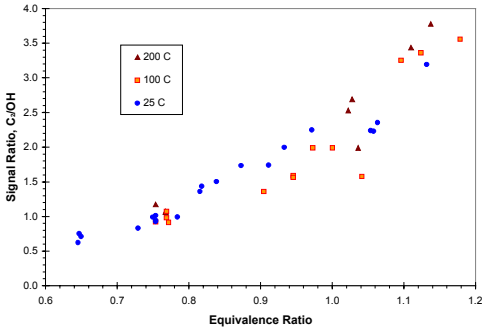

Figure 16. Effect of inlet air temperature on C_2*/OH* emission ratio.

The trends found here agree in general with the recently reported data by Kojima *et al.*,[14] taken in a laminar, premixed, methane-air flame. The most significant difference is the much higher sensitivity to ϕ for the C_2*/OH* ratio in the methane-air flame. This is likely due to the limited chemical pathways for production of the C_2 from CH_4 (which lacks any C-C bonds), especially in lean mixtures. In the combustion of a complex hydrocarbon such as n-heptane, there are more pathways that lead to C_2* in both lean and rich mixtures, and thus a correspondingly smaller dependence on equivalence ratio. It should also be noted that the methane data were acquired for equivalence ratios from 0.9 to 1.5, and the radical emission ratios become less sensitive to equivalence ratio changes for ϕ>1.35. Due to the differences between the two systems, it is not clear if this trend holds for the n-heptane results.

Local Emission Ratios

The results presented thus far show a correlation between *overall* equivalence ratio and the ratio of the

"volume" integrated chemiluminescence signals. An important question remains, specifically, whether a similar correlation holds for smaller ("local") regions of the combustor. As previously stated, the local equivalence ratio at any point within the combustor is unknown due to the non-premixed and turbulent nature of the system. However, we can examine the variation of the local emission ratio with downstream distance, and attempt to apply the correlation found above to the result.

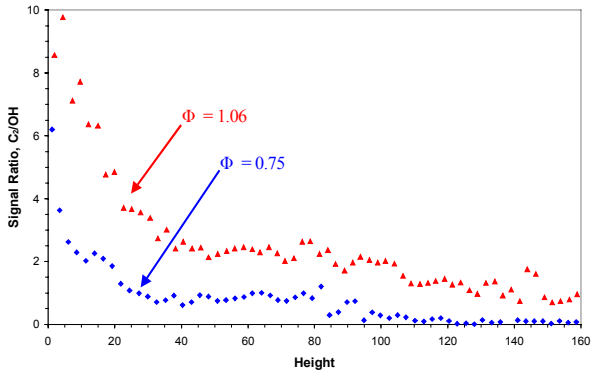

Figure 17. Variation of the C_2*/OH* emission ratio with height above the flameholder.

Figure 17 shows the local C_2*/OH* emission ratio at each height in the flame for different equivalence ratios, taken from the data similar to that shown in Figures 7-10. The emission ratio is highest near the exit of the flameholder, indicative of a richer reaction zone there. Recall that the primary mixture exiting the flameholder has an equivalence ratio that is roughly three times the overall equivalence ratio. Farther downstream, more secondary air mixes with the primary flow, lowering the local equivalence ratio. Thus, the roughly monotonic decrease in the emission ratio with increasing height indicates a monotonically decreasing equivalence ratio of the reaction zone. The results also indicate that a large portion of the flame zone, generally 40-80 mm downstream of the flameholder, has a nearly uniform emission ratio, indicating a nearly uniform equivalence ratio. These observations are consistent with the likely mixing processes in the combustor.

Figure 18 shows the result of applying the linear correlation indicated in Figure 13 to the local emission data, and extrapolating as necessary. For example at an overall equivalence ratio of 0.75, the local equivalence ratio just above the flameholder is estimated to be 1.8, based on a C_2*/OH* emission ratio of ~6. This compares to the expected primary flow equivalence ratio of 2.3 (3× the overall ϕ). It is reasonable to assume that the local reaction zone equivalence ratio is even leaner than this primary flow value. Firstly, there is evidence that not all of the fuel droplets are evaporated by the flameholder lip. Secondly, the recirculation zone near the flameholder would mix some of the secondary air into the primary flow, lowering the equivalence ratio further. However, based on the results by Kojima *et al.*[14], it is also likely that the linear extrapolation of the integrated C_2*/OH* results beyond the measured limit of ϕ=1.2 overestimates the sensitivity of the emission ratio for rich mixtures. Thus the predicted local equivalence ratio of 1.8 at the flameholder tip would likely be lower than the actual value.

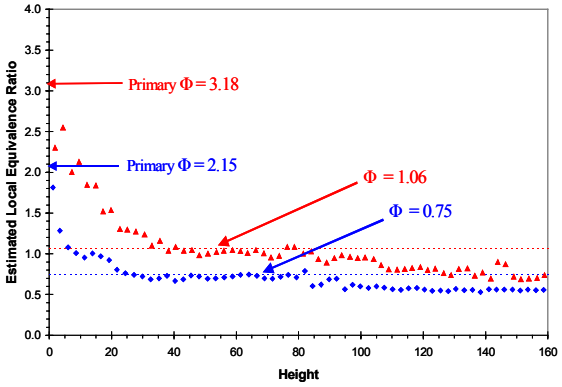

Figure 18. Estimated local reaction zone equivalence ratio as a function of height based on C_2*/OH* emission ratio correlation.

For the same flame with an overall ϕ=0.75, the C_2*/OH* emission ratio at the end of the reaction zone is ~0.8, corresponding to a local equivalence ratio of ~0.6. This value is below the overall equivalence ratio of the combustor, as expected. Because the combustion zone low in the flame burns richer than the overall equivalence ratio, the final reaction zone must be leaner. While these comparisons do not prove that the correlation derived from the integrated results is valid for local equivalence ratio sensing, they do lend credence to this hypothesis.

Summary and Conclusions

The optical emissions from a swirling, non-premixed, liquid-fueled (n-heptane) combustor were measured using two systems. Initial measurements were taken using a monochromator system configured to record at a high spectral resolution. An imaging spectrometer system was then used to make simultaneous measurements of the ultraviolet and visible emission (280 – 550 nm), including that from OH*, CH*,

and C_2*. The reduced spectral resolution of the imaging system is more typical of the likely resolution of a practical, on-board, optical engine sensor. Several interesting results were obtained that can be used to provide useful information on the combustor.

Both OH* and CH* signals, normalized by the fuel flow rate, remained relatively constant over a range of lean equivalence ratios, indicating that in these ranges they can be accurately used as an indication of overall heat release (or heat release rate). However since these ranges are relatively small (from the lower range of the measurements ϕ=0.64 up to ϕ=0.9 for OH*, and 0.75<ϕ<0.9 for CH*), it would be necessary either to verify that the flame is burning within the valid range of equivalence ratios or to account for the variation in emissions once outside the valid range. In either case, there would be a need to monitor the equivalence ratio. In addition, the downstream emission from OH* was found to be larger relative to its peak than was the case for CH* and C_2*. If the source of the OH* is thermal, then this could provide a means of monitoring temperature in the post-reaction zone of the combustor.

The ratios of the radical emissions integrated over the combustor volume were found to vary monotonically with the overall equivalence ratio of the combustor. Furthermore, over the range of equivalence ratios tested, 0.6 to 1.3, the emission ratios varied nearly linearly with ϕ. The emission ratio of C_2* to OH* exhibited the largest slope sensitivity of the three ratios studied. The results from the broadband detection system, when corrected for the background, agreed well with the narrowband detection results. Even without correction, however, the broadband system still was able to produce a nearly linear relationship between emission ratios and equivalence ratio, albeit with a reduced sensitivity.

The correlation of the C_2*/OH* emission with overall equivalence ratio was applied to local emission ratios to estimate local reaction zone equivalence ratios along the length of the combustor. Within the limits of the extrapolation required to extend the correlation beyond the measured values of ϕ, the results agreed well with equivalence ratio expected at the exit of the flame holder. They also indicated that the reaction zone became progressively leaner downstream, with a nearly uniform region in the central region of the combustor, and a final equivalence ratio at the flame tip that was leaner than the overall ϕ. While more effort is required to test the accuracy of applying the globally based correlation to local properties, such ability to determine the local equivalence ratio would permit an optical emission sensor system to more accurately monitor heat release using OH* or CH* over a broad range of equivalence ratios.

In conclusion, the results indicate that a passive, optical sensor would be capable of gathering pertinent information for use in an intelligent combustor/engine control or health monitoring system. A properly designed system of sensors would be able to remotely monitor a large area of the combustor to determine such information as the presence of a flame, the local equivalence ratio, local heat release and possibly temperature. The sensor system would require a minimum of two sensors, each monitoring a different emission band. If the combustor was likely to have significant broadband background, the use of additional sensors to monitor the background in the vicinity of each emission band would increase the sensitivity and accuracy of the sensor system.

Acknowledgments

Portions of this work were supported by Innovative Scientific Solutions, Inc. (technical monitor, Dr. Geoffrey Sturgess) and the Air Force Research Laboratory (contract F33615-99-C-2978, technical monitor, Dr. Carlos Arana) under a Department of Defense Phase I Small Business Technology Transfer Program, in part by General Electric Power Systems (technical monitors, Dr. S. Sharma and Dr. D. Ozgur), and in part by the US Air Force Office of Scientific Research (contract F49620-99-1-0142, technical monitor Dr. Mitat Birkan).

References

[1]Wei Yang, Nohava, T., Krishnankutty, S., Torreano, R., McPherson, S., and Marsh, H., "GaN/AlGaN UV photodiodes and phototransistors," Proceedings of the SPIE, Vol. 3287, 1998, pp.188-197.

[2]Brown, D. M., Downey, E., Kretchmer, J., Mickon, G., Shu, E., and Schneider, D., "SiC Flame Sensors for Gas Turbine Control Systems," Solid-State Electronics, Vol. 42, No.5, 1998, pp.755-760.

[3]Samaniego, J.M., Egolfopoulos, F.N., and Bowman, C.T. "CO_2* Chemiluminescence in Premixed Flames," Combustion Science and Technology, Vol. 109, 1995, pp. 183-203.

[4]Mizutani, Y., Nakabe, K., Matsumoto, Y., Saeki, T., and Matsui, T., "Processing of Luminescent Radical Images for Flame Diagnostics," JSME Int. J. Series II Vol. 32 No. 3, 1989, pp. 455-463.

[5]Gaydon, A.G. and Wolfhard, H.G., Flames: Their Structure, Radiation, and Temperature. Fourth edition, Chapman and Hall, 1978.

[6]Jensen, R.J. and Fisher, S.C., "Nonintrusive Temperature Measurements in SSME Preburner Element Flowfields," 23rd JANNAF Combustion Meeting, Vol. 1, 1986, pp 663-640.

[7]Roby, R. J., Reaney, J .E., and Johnsson, E. L., "Detection of Temperature and Equivalence Ratio in Turbulent Premixed Flames Using Chemiluminescence," Proceedings of the 1998 Int. Joint Power Generation Conference, Vol. 1, 1998, 593-602.

[8]Keller, J.O. and Saito, K., "Measurements of the Combusting Flow in a Pulse Combustor," Combustion Science and Technology, Vol. 53, 1987, pp. 137-163.

[9]Lawn, C.J., "Distributions of Instantaneous Heat Release by the Cross-Correlation of Chemiluminescent Emissions," Combustion and Flame, Vol. 132, 2000, pp. 227-240.

[10]Kojima, J., Ikeda, Y., and Nakajima, T., "Measuring Local OH* to Analyze Flame Front Movement in a Turbulent Premixed Flame," 35th AIAA/ASME/ASEE Joint Propulsion Conference and Exhibit, 1999.

[11]Ikeda, Y., Kojima, J., and Nakajima, T., "Measurement of the Local Flame-Front Structure of Turbulent Premixed Flames by Local Chemiluminescence."

[12]Roby, R.J., Hamer, A.J., Johnsson, E.L., Tilstra, S.A., and Burt, T.J., "Improved Method for Flame Detection in Combustion Turbines, Transactions of the ASME, Vol. 117, 1995, pp. 332 –340.

[13]Dandy, D. S. and Vosen, S. R., "Numerical and Experimental Studies of Hydroxyl Radical Chemiluminescence in Methane-Air Flame," Combustion Science and Technology, Vol. 82, 1992, pp. 131-150.

[14]Kojima, J., Ikeda, Y., and Nakajima, T., "Spatially Resolved Measurement of OH*, CH*, and C_2* Chemiluminescence in the Reaction Zone of Laminar Methane/Air Premixed Flames."

[15]Kappei, F., Lee, J. Y., Johnson, C. E., Lubarsky, E., Neumeier, Y., and Zinn, B. T., "Investigation of Oscillatory Combustion Processes in an Actively Controlled Liquid Fuel Combustor," Paper 2000-3348 AIAA/ASME/SAE/ASEE 36th Joint Propulsion Conference and Exhibit, Huntsville, AL, July 16-19, 2000.